Journal of Guidance, Control, and Dynamics
Vol. 28, No. 5, September–October 2005

Multiple Impedance Control for Space Free-Flying Robots

S. Ali A. Moosavian and Rambod Rastegari
K. N. Toosi University of Technology, 16579 Tehran, Iran
and
Evangelos Papadopoulos
National Technical University of Athens, 15780 Athens, Greece

To increase the mobility of on-orbit robotic systems, space free-flying robots (SFFR), in which one or more manipulators are mounted on a thruster-equipped base, have been proposed. Unlike fixed-based manipulators, the robotic arms of SFFR are dynamically coupled with each other and the free-flying base; hence, the control problem becomes more challenging. The multiple impedance control (MIC) is developed to manipulate space objects by multiple arms of SFFR. The MIC law is based on the concept of designated impedances and enforces them at various system levels, that is, the free-flying base, all cooperating manipulators, and the manipulated object itself. The object can include an internal angular momentum source, as is the case in most satellite manipulation tasks. The disturbance rejection characteristic of this algorithm is also studied. The result of this analysis reveals that the effect of disturbances substantially reduces through appropriate tuning of the controller mass matrix gain. A system of three manipulators mounted on a free-flying base is simulated in which force and torque disturbances are exerted at several points. The system dynamics is developed symbolically, and the controlled system is simulated. The simulation results reveal the merits of the MIC algorithm in terms of smooth performance, that is, negligible small tracking errors in the presence of impacts as a result of contact with the obstacles and significant disturbances.

S. Ali A. Moosavian received his B.S. degree in 1986 from Sharif University of Technology and the M.S. degree in 1990 from Tarbiat Modaress University (both in Tehran) and his Ph.D. degree in 1996 from McGill University, all in mechanical engineering. He has been an Assistant Professor with the Mechanical Engineering Department at K.N. Toosi University of Technology (Tehran) since 1997. He teaches courses in the areas of robotics, dynamics, automatic control, and analysis and synthesis of mechanisms. His research interests are in the areas of dynamics modeling and motion/impedance control of terrestrial and space robotic systems. He has published about 40 papers in journals and conference proceedings. He is one of the founders of the ARAS Research Center for Design, Manufacturing and Control of Robotic Systems, and Automatic Machineries. E-mail: moosavian@kntu.ac.ir.

Rambod Rastegari received his B.S. degree in 1996 from Sharif University of Technology and M.S. degree in 1999 from K.N. Toosi University of Technology (both in Tehran) in mechanical engineering. He is currently a Ph.D. student at the Mechanical Engineering Department of K.N.T. University of Technology. His dissertation subject is in the areas of dynamics modeling and control of mobile robotic systems with the emphasis on space free-flying robots.

Evangelos Papadopoulos received his Diploma from the National Technical University of Athens (NTUA) in 1981 and his M.S. and Ph.D. degrees from the Massachusetts Institute of Technology (MIT) in 1983 and 1991, respectively, all in mechanical engineering. From 1985 to 1987, he was an analyst with the Hellenic Navy, Athens, Greece. In 1991 he was appointed a Lecturer at the Department of Mechanical Engineering at MIT. He then joined McGill University and the Centre for Intelligent Machines (CIM) as an Assistant Professor and was tenured in 1997. Currently, he is an Associate Professor with the Mechanical Engineering Department at the NTUA. He teaches courses in the areas of systems, controls, mechatronics, and robotics. His research interests are in the area of robotics, including space, mobile, and underwater robotics, modeling and control of dynamic systems, haptic devices, mechatronics, and design. In 2003, he served as a Guest Editor for the Advances in Robot Dynamics and Control issue of the *ASME/IEEE Transactions on Mechatronics*. He has published more than 85 papers in journals and conference proceedings. He is a Senior Member of the AIAA and of the Institute of Electrical and Electronics Engineers, and a member of the American Society of Mechanical Engineers, the NYAS, the Technical Chamber of Greece, and Sigma Xi. E-mail: egpapado@central.ntua.gr.

Received 19 April 2004; revision received 13 July 2004; accepted for publication 20 September 2004.

Nomenclature

$\boldsymbol{C}$ = vector that contains all gravity and nonlinear velocity terms of the dynamics model, where $\hat{\boldsymbol{C}}$ or $\tilde{\boldsymbol{C}}$ corresponds to the one in the task space, and a superscript i refers to the ith manipulator

$\boldsymbol{e}, \tilde{\boldsymbol{e}}$ = vector of tracking errors, where a subscript is used for a particular variable, for example, $\boldsymbol{e}_\omega$ is the error in angular velocity, and a superscript i corresponds to the ith manipulator

$\boldsymbol{F}_c$ = 6×1 vector that contains the forces/moments applied on an acquired object caused by contact with the environment

$\hat{\boldsymbol{F}}_c$ = estimated value of contact force $\boldsymbol{F}_c$

$\boldsymbol{F}_e$ = $6n \times 1$ vector that contains all end-effector forces/torques applied on an acquired object, where $\boldsymbol{F}_e^{(i)}$ is a $6\infty 1$ vector corresponding to the ith end effector

$\boldsymbol{F}_{e_{\mathrm{req}}}$ = required end-effector forces/torques to be applied on an acquired object, where $\boldsymbol{F}_{e_{\mathrm{req}}}^{(i)}$ is a $6\infty 1$ vector corresponding to the ith end effector

$\boldsymbol{F}_G$ = required force for moving an internal angular momentum source along with the acquired object motion

$\boldsymbol{F}_\omega$ = 6×1 vector that contains nonlinear velocity terms in an acquired object dynamics equations

$\boldsymbol{F}_0$ = 6×1 vector that contains external forces/moments (other than contact and end-effector ones) applied on an acquired object

$\boldsymbol{f}_c, \boldsymbol{n}_c$ = resultant force (torque) applied on an acquired object as a result of contact, where $\boldsymbol{n}_c$ includes moment of $\boldsymbol{f}_c$ about the object c.m.

$\boldsymbol{f}_e^{(i)}, \boldsymbol{n}_e^{(i)}$ = ith end-effector force (torque) exerted on an acquired object

$\boldsymbol{f}_0, \boldsymbol{n}_0$ = vector of external forces (torques), other than contact and end-effector ones, applied on an acquired object (including gravity effects), where $\boldsymbol{n}_0$ includes moment of $\boldsymbol{f}_0$ about the object c.m.

$\boldsymbol{G}$ = $6 \times 6n$ grasp matrix that maps the vector of all end-effector forces/torques to an acquired object dynamics equations

$\boldsymbol{G}^{\#}$ = weighted pseudoinverse of the grasp matrix $\boldsymbol{G}$

$\boldsymbol{H}$ = positive-definite mass matrix of the system, where $\hat{\boldsymbol{H}}$ or $\tilde{\boldsymbol{H}}$ corresponds to the one in the task space, and a superscript i refers to the ith manipulator

i_f = number of applied force/torque vectors on a body

$\boldsymbol{J}_C$ = square Jacobian matrix that relates the output speeds to the generalized ones, where a superscript i corresponds to the ith manipulator

$\boldsymbol{J}_i^{(m)}$ = $6 \times \boldsymbol{N}$ Jacobian matrix that relates the generalized velocities $\dot{\boldsymbol{q}}$ to the linear velocity $\dot{\boldsymbol{R}}_i$ and angular velocity $\boldsymbol{\omega}_i^{(m)}$ of the exerted body

$\boldsymbol{J}_Q$ = $N \times N$ Jacobian matrix that relates the vector of actuator forces/torques to the vector of generalized forces

$\boldsymbol{K}_p, \boldsymbol{K}_d$ = control gain matrices

$\boldsymbol{k}_e$ = stiffness matrix of a remote-center-compliance unit

$\tilde{\boldsymbol{k}}_p, \tilde{\boldsymbol{k}}_d, \tilde{\boldsymbol{M}}_{\mathrm{des}}$ = block-diagonal $N \times N$ control gain and desired mass matrices, composed of the corresponding 6×6 matrices that define the impedance law for the acquired object

k_w = stiffness coefficient of an obstacle located at x_w, in a unilateral study

$\boldsymbol{L}_G$ = angular momentum of an internal source about the acquired object c.m.

$\boldsymbol{L}_s$ = angular momentum of an internal source about its own c.m.

$\boldsymbol{M}$ = 6×6 mass matrix for an acquired object

$\boldsymbol{M}_{\mathrm{des}}$ = acquired object desired mass matrix, in the impedance law

$\boldsymbol{M}_G$ = required moment for moving an internal angular momentum source along with the acquired object motion

$m_{\mathrm{obj}}, \boldsymbol{I}_G$ = acquired object mass and its moment of inertia about c.m.

m_s = mass of an internal angular momentum source that is not included in the acquired object mass m_{obj}

N = system total degrees of freedom (DOF)

N_m = number of joints (single DOF), for the mth manipulator

n = number of manipulators or appendages, for a system of multiple manipulators

n_f = number of disturbing torque/force applied on the ith link of the mth manipulator

$\boldsymbol{p}_s$ = linear momentum of an internal angular momentum source, inside an acquired object

$\boldsymbol{Q}$ = vector of generalized forces, where $\tilde{\boldsymbol{Q}}$ corresponds to the one in the task space and a superscript i refers to the ith manipulator

$\tilde{\boldsymbol{Q}}_{\mathrm{app}}$ = applied controlling force (expressed in the task space), where a superscript i refers to the ith manipulator, $= \tilde{\boldsymbol{Q}}_m + \tilde{\boldsymbol{Q}}_f$

$\boldsymbol{Q}_{\mathrm{dist}}$ = vector of generalized disturbing forces, where $\tilde{\boldsymbol{Q}}_{\mathrm{dist}}$ corresponds to the one in the task space

$\boldsymbol{Q}_{\mathrm{dist}_{ij}}^{(m)}$ = jth disturbing torque/force applied on the ith link of the mth manipulator

$\tilde{\boldsymbol{Q}}_f$ = required force to be applied on the manipulated object by the end effector, where a superscript i refers to the ith manipulator

$\tilde{\boldsymbol{Q}}_m$ = applied controlling force concerning the motion of the end effector, where a superscript i refers to the ith manipulator

$\tilde{\boldsymbol{Q}}_{\mathrm{react}}$ = reaction force (expressed in the task space) on the end effector, where a superscript i refers to the ith manipulator

$\boldsymbol{q}, \dot{\boldsymbol{q}}, \ddot{\boldsymbol{q}}$ = $N \times 1$ vector of generalized coordinates, and its rate, where a superscript i corresponds to the ith manipulator

$\boldsymbol{R}_{C_0}, \dot{\boldsymbol{R}}_{C_0}, \ddot{\boldsymbol{R}}_{C_0}$ = inertial position, velocity, and acceleration of the spacecraft c.m., where the components are expressed as x_0, y_0, z_0, etc.

$\boldsymbol{R}_{\mathrm{CM}}, \dot{\boldsymbol{R}}_{\mathrm{CM}}, \ddot{\boldsymbol{R}}_{\mathrm{CM}}$ = inertial position, velocity, and acceleration of the system c.m., where the components are expressed as x_{CM}, y_{CM}, z_{CM}, etc.

$\boldsymbol{r}_e^{(i)}$ = position vector of the ith end effector with respect to the object c.m.

$\boldsymbol{r}_s$ = position vector of the angular momentum source c.m. with respect to the object c.m.

$\boldsymbol{S}_{\mathrm{obj}}$ = 3×3 matrix, which relates the angular velocity of an acquired object to the Euler angle rates

$\boldsymbol{U}_{f_c}$ = $N \times 6$ matrix, composed of $(n+1)$ 6×6 identity matrices

$\boldsymbol{v}_s$ = inertial linear velocity of the internal angular momentum source c.m.

$\boldsymbol{X}$ = 6×1 vector $[\boldsymbol{X} = (\boldsymbol{x}_G^T, \boldsymbol{\delta}_{\mathrm{obj}}^T)^T]$, which contains the c.m. position, and Euler angles of an acquired object, where $\dot{\boldsymbol{X}}$ and $\ddot{\boldsymbol{X}}$ are its rates, and $\boldsymbol{X}_{\mathrm{des}}$, $\dot{\boldsymbol{X}}_{\mathrm{des}}$, and $\ddot{\boldsymbol{X}}_{\mathrm{des}}$ are the desired ones

$\tilde{\boldsymbol{X}}$ = vector of controlled variables and its rates, where $\tilde{\boldsymbol{X}}_{\text{des}}$, $\dot{\tilde{\boldsymbol{X}}}_{\text{des}}$, and $\ddot{\tilde{\boldsymbol{X}}}_{\text{des}}$ refer to the desired ones and a superscript i corresponds to the ith manipulator

$\boldsymbol{x}_E^{(m)}, \dot{\boldsymbol{x}}_E^{(m)}$ = mth end-effector inertial position and velocity vector; $\boldsymbol{x}_E^{(m)} = [x_E^{(m)}, y_E^{(m)}, z_E^{(m)}]$, etc.

$\boldsymbol{x}_G, \dot{\boldsymbol{x}}_G, \ddot{\boldsymbol{x}}_G$ = inertial position, velocity, and acceleration of an acquired object c.m.

Δt = time step used in the estimation procedure

$\boldsymbol{\delta}_E^{(m)}$ = set of Euler angles that describes the mth end-effector orientation, $= [\alpha_E^{(m)}, \beta_E^{(m)}, \gamma_E^{(m)}]$, and becomes a single angle $\boldsymbol{\delta}_E^{(m)}$ in planar motion

$\boldsymbol{\delta}_{\text{obj}}$ = set of Euler angles that describes an acquired object attitude

$\boldsymbol{\delta}_0$ = set of Euler angles that describes the spacecraft attitude, $= (\alpha_0, \beta_0, \gamma_0)$

$\boldsymbol{\theta}$ = $K_n \times 1$ column vector ($K_n = \sum_{m=1}^{n} N_m$), which contains all joint angle vectors, $[\boldsymbol{\theta}^{(1)^T}, \boldsymbol{\theta}^{(2)^T}, \ldots, \boldsymbol{\theta}^{(n)^T}]^T$

$\boldsymbol{\theta}^{(m)}$ = $N_m \times 1$ column vector that contains the joint angles of the mth manipulator, where $\theta_i^{(m)}$ refers to its ith component (joint)

${}^m\boldsymbol{\omega}_E^{(m)T}$ = angular velocity of the mth end effector expressed in its own body-fixed frame

$\boldsymbol{\omega}_{\text{obj}}, \dot{\boldsymbol{\omega}}_{\text{obj}}$ = acquired object angular velocity and acceleration

$\boldsymbol{0}$ = zero matrix

$\boldsymbol{1}$ = identity matrix

I. Introduction

ROBOTIC systems are expected to play an important role in space applications, for example, in the servicing, construction, and maintenance of space structures on orbit. For instance, robotic systems can be used to inspect, capture, and repair or refuel damaged satellites. Ultimately, coordinated teams of robots might deploy, transport, and assemble structural modules for a large space structure.[1] Space free-flying robots (SFFR) are robotic systems that include an actuated relatively small base equipped with one or more manipulators (Fig. 1). Distinct from fixed-based manipulators, the base of SFFR responds to dynamic reaction forces caused by manipulator motions. To control such a system, it is essential to consider the dynamic coupling between the manipulators and the base, by developing proper kinematics/dynamics model for the system.[2–4] Motion control of SFFR has been studied by various researchers.[5–10] Also, coordinated control of free-flying base and its multiple manipulators during capture or manipulation of objects has received attention.[11–15]

To control interaction forces and system response during contact, force or impedance control strategies are required. Hybrid position/force control has been the basic strategy of several proposed implementations.[16,17] Nevertheless, because of several control mode switchings during most tasks, particularly in unexpected situations, hybrid control does not provide an efficient interface. (Control of a robot in free motions and contact tasks are considered as two different control modes. In free motion, a position control algorithm can be employed, whereas in contact tasks the interaction with the environment should be managed using force/impedance algorithms. Most tasks include both free motions and contact tasks, that is, tracking a desired path and interaction with the environment at specific points, for example, insertion of a pin in a hole. Therefore, switching between the two modes is required if hybrid position/force approach is used.) Impedance control provides compliant behavior of a single manipulator in dynamic interaction with its environment.[18] An impedance controller enforces a relationship between external force(s)/torque(s) acting on the environment, and the position, velocity, and acceleration error of the end effector. Adaptive schemes have been presented to make impedance control capable of tracking a desired contact force, which has been described as the main shortcoming of impedance control in an unknown environment.[19,20] Optimizing the regulation of impedance control from the viewpoint of both the transient and steady-state responses, using the concept of impedance matching to choose optimal parameters has been proposed.[21] A Cartesian impedance controller has been presented to overcome the main problems encountered in fine manipulation, that is, effects of the friction (and unmodeled dynamics) on robot performance and occurrence of singularity conditions.[22–24] Experimental and simulation investigations into the performance of impedance control implemented on elastic joints have shown the benefits of using this control strategy in compensating undesirable effects caused by system flexibilities.[25]

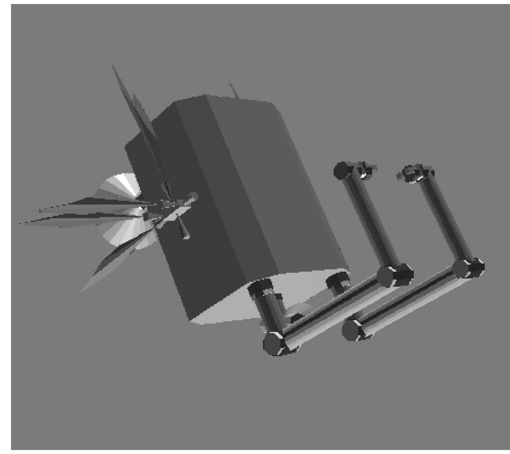

Fig. 1 SFFR with multiple manipulators.

Object impedance control (OIC) has been developed for robotic arms manipulating a common object.[26] The OIC enforces a designated impedance not for an individual manipulator endpoint, but for the manipulated object itself. A combination of feedforward and feedback strategies is employed to make the object behave as a reference impedance. However, it has been recognized that applying the OIC to the manipulation of a flexible object can lead to instability.[27] It was suggested that either increasing the desired mass parameters or filtering the frequency content of the estimated contact force might solve the instability problem. Multiple impedance control (MIC) is an algorithm that has been developed for several cooperating robotic systems manipulating a common object.[28,29]

In this paper, the MIC law is studied in the context of space robotic systems. The MIC formulation is extended to impose a reference impedance to all elements of a SFFR, including its free-flying base, the manipulator endpoints, and the manipulated object. It is assumed that the manipulated object includes an internal angular momentum source, as it is the case in most satellite manipulation tasks. The effect of torque/force disturbances applied on different points of the system is studied next. Results show that through appropriate tuning of the MIC mass matrix gain the effect of disturbances is substantially reduced. Next, a system of three manipulators mounted on a space free flyer is simulated during a planar maneuver. To consider practical aspects, it is assumed that a remote center compliance is attached to the second end effector and that the system is subjected to significant force and torque disturbances at several points. Also, the desired trajectories are planned such that the object comes into contact with an obstacle. Simulation results reveal the merits of the MIC algorithm in terms of its smooth performance, that is, resulting in negligible small tracking errors in the presence of both impacts caused by contact with the environment and imposed disturbances and in a soft stop at the obstacle position following the contact.

II. MIC Law for Space Free Flyers

A. System Dynamics

In this section, a brief review of the dynamics modeling of space free-flying robots with multiple arms is presented (for more details, see Ref. 30). Assuming that the system consists of rigid elements, the vector of generalized coordinates can be chosen as

$$\boldsymbol{q} = \left(\boldsymbol{R}_{\text{CM}}^T, \boldsymbol{\delta}_0^T, \boldsymbol{\theta}^T\right)^T \tag{1}$$

where

$$\boldsymbol{\theta} = \left[\boldsymbol{\theta}^{(1)^T}, \ldots, \boldsymbol{\theta}^{(n)^T}\right]^T \tag{2}$$

which is a $K_n \times 1$ column vector where $\boldsymbol{\theta}^{(m)}$ is an $N_m \times 1$ column vector that contains the joint angles of the mth manipulator, and

$$K_n = \sum_{m=1}^{n} N_m$$

The vector of output (controlled) variables is defined as

$$\tilde{\boldsymbol{X}} = \left[\boldsymbol{R}_{C_0}^T, \boldsymbol{\delta}_0^T, \boldsymbol{X}_E^{(1)T}, \boldsymbol{\delta}_E^{(1)T}, \ldots, \boldsymbol{X}_E^{(n)T}, \boldsymbol{\delta}_E^{(n)T}\right] \tag{3}$$

which is a $K_n + 6$ column vector. Applying the general Lagrangian formulation,[31] or any other method, the equations of motion can be obtained and expressed in the task space, that is, in terms of the output coordinates $\tilde{\boldsymbol{X}}$, as

$$\tilde{\boldsymbol{H}}(\boldsymbol{q})\ddot{\tilde{\boldsymbol{X}}} + \tilde{\boldsymbol{C}}(\boldsymbol{q}, \dot{\boldsymbol{q}}) = \tilde{\boldsymbol{Q}} \tag{4}$$

where $\tilde{\boldsymbol{H}}$ describes the system mass matrix, $\tilde{\boldsymbol{C}}$ contains all nonlinear terms, and $\tilde{\boldsymbol{Q}}$ describes the vector of generalized forces in the task space.

To develop the MIC law, the vector of generalized forces $\tilde{\boldsymbol{Q}}$ is written as

$$\tilde{\boldsymbol{Q}} = \tilde{\boldsymbol{Q}}_{\text{app}} + \tilde{\boldsymbol{Q}}_{\text{react}} = \tilde{\boldsymbol{Q}}_m + \tilde{\boldsymbol{Q}}_f + \tilde{\boldsymbol{Q}}_{\text{react}} \tag{5}$$

where $\tilde{\boldsymbol{Q}}_{\text{app}}$ is the applied controlling force consisting of the force that corresponds to the motion of the system $\tilde{\boldsymbol{Q}}_m$ and of the required force to be applied on the manipulated object by the end effectors $\tilde{\boldsymbol{Q}}_f$. To determine these terms, the object dynamics is considered next.

B. Object Dynamics

The equations of motion for a rigid object can be written as

$$\boldsymbol{M}\ddot{\boldsymbol{X}} + \boldsymbol{F}_\omega = \boldsymbol{F}_c + \boldsymbol{F}_0 + \boldsymbol{G}\boldsymbol{F}_e \tag{6}$$

An active object is assumed, that is, the object includes an internal angular momentum source, as shown in Fig. 2. The preceding forces, the mass matrix $\boldsymbol{M}$ and the grasp matrix $\boldsymbol{G}$, will be detailed in the following.

The linear momentum of the source $\boldsymbol{p}_s$ can be written as

$$\boldsymbol{p}_s = m_s \boldsymbol{v}_s = m_s(\dot{\boldsymbol{x}}_G + \boldsymbol{\omega}_{\text{obj}} \times \boldsymbol{r}_s) \tag{7}$$

The required force for moving the internal angular momentum source along with the object motion $\boldsymbol{F}_G$ can be written as

$$\boldsymbol{F}_G = \dot{\boldsymbol{p}}_s = \frac{\mathrm{d}}{\mathrm{d}t} m_s \boldsymbol{v}_s \tag{8}$$

Therefore, differentiation of Eq. (7) and substitution of the result into Eq. (8) yields

$$\boldsymbol{F}_G = m_s[\ddot{\boldsymbol{x}}_G + \dot{\boldsymbol{\omega}}_{\text{obj}} \times \boldsymbol{r}_s + \boldsymbol{\omega}_{\text{obj}} \times (\boldsymbol{\omega}_{\text{obj}} \times \boldsymbol{r}_s)] \tag{9}$$

which has to be included in Eq. (6) for linear motion.

For the object angular motion, based on the translation theorem for angular momentum,[31] it can be written

$$\boldsymbol{L}_G = \boldsymbol{L}_s + \boldsymbol{r}_s \times \boldsymbol{p}_s \tag{10}$$

Therefore, the required moment for moving the internal angular momentum source along with the object motion, written about the object center of mass, is

$$\boldsymbol{M}_G = \dot{\boldsymbol{L}}_G + \dot{\boldsymbol{x}}_G \times \boldsymbol{p}_s \tag{11}$$

Assuming that $\boldsymbol{L}_s$ has a constant magnitude, as it is for an internal angular momentum source, results in

$$\boldsymbol{M}_G = \boldsymbol{\omega}_{\text{obj}} \times \boldsymbol{L}_s + \frac{\mathrm{d}}{\mathrm{d}t}(\boldsymbol{r}_s \times \boldsymbol{p}_s) + \dot{\boldsymbol{x}}_G \times m_s(\dot{\boldsymbol{x}}_G + \boldsymbol{\omega}_{\text{obj}} \times \boldsymbol{r}_s) \tag{12a}$$

Calculating different terms of Eq. (12), and substituting the results back into the equation, yields

$$\boldsymbol{M}_G = \boldsymbol{\omega}_{\text{obj}} \times \boldsymbol{L}_s + m_s \boldsymbol{r}_s \times [\ddot{\boldsymbol{x}}_G + \dot{\boldsymbol{\omega}}_{\text{obj}} \times \boldsymbol{r}_s + \boldsymbol{\omega}_{\text{obj}} \times (\boldsymbol{\omega}_{\text{obj}} \times \boldsymbol{r}_s)] \tag{12b}$$

which has to be included in Eq. (6) for angular motion as

$$\begin{aligned} &\boldsymbol{I}_G \dot{\boldsymbol{\omega}}_{\text{obj}} + \boldsymbol{\omega}_{\text{obj}} \times \boldsymbol{I}_G \boldsymbol{\omega}_{\text{obj}} + \boldsymbol{\omega}_{\text{obj}} \times \boldsymbol{L}_s + m_s \boldsymbol{r}_s \\ &\quad \times [\ddot{\boldsymbol{x}}_G + \dot{\boldsymbol{\omega}}_{\text{obj}} \times \boldsymbol{r}_s + \boldsymbol{\omega}_{\text{obj}} \times (\boldsymbol{\omega}_{\text{obj}} \times \boldsymbol{r}_s)] \\ &\quad = \boldsymbol{n}_c + \boldsymbol{n}_0 + \sum_{i=1}^{m} \boldsymbol{r}_e^{(i)} \times \boldsymbol{f}_e^{(i)} + \sum_{i=1}^{m} \boldsymbol{n}_e^{(i)} \end{aligned} \tag{13}$$

Now all of these terms can be put together and written in the matrix form of Eq. (6), where

$$\boldsymbol{M} = \begin{bmatrix} (m_{\text{obj}} + m_s)\mathbf{1}_{3\times 3} & -m_s[\boldsymbol{r}_s]^\times \boldsymbol{S}_{\text{obj}} \\ m_s \boldsymbol{S}_{\text{obj}}^T [\boldsymbol{r}_s]^\times & \boldsymbol{S}_{\text{obj}}^T(\boldsymbol{I}_G + \boldsymbol{I}_s)\boldsymbol{S}_{\text{obj}} \end{bmatrix} \tag{14a}$$

$$\boldsymbol{I}_s = m_s \begin{bmatrix} r_{s_y}^2 + r_{s_z}^2 & -r_{s_x} r_{s_y} & -r_{s_x} r_{s_z} \\ -r_{s_x} r_{s_y} & r_{s_x}^2 + r_{s_z}^2 & -r_{s_y} r_{s_z} \\ -r_{s_x} r_{s_z} & -r_{s_y} r_{s_z} & r_{s_x}^2 + r_{s_y}^2 \end{bmatrix} \tag{14b}$$

$$\boldsymbol{F}_c = \begin{Bmatrix} \boldsymbol{f}_c \\ \boldsymbol{S}_{\text{obj}}^T \boldsymbol{n}_c \end{Bmatrix} \quad \boldsymbol{F}_0 = \begin{Bmatrix} \boldsymbol{f}_0 \\ \boldsymbol{S}_{\text{obj}}^T \boldsymbol{n}_0 \end{Bmatrix} \quad \boldsymbol{F}_e^{(i)} = \begin{Bmatrix} \boldsymbol{f}_e^{(i)} \\ \boldsymbol{n}_e^{(i)} \end{Bmatrix}_{6\times 1} \tag{14c}$$

$$\boldsymbol{F}_e = \begin{Bmatrix} \boldsymbol{F}_e^{(1)} \\ \vdots \\ \boldsymbol{F}_e^{(n)} \end{Bmatrix}_{6n\times 1} \tag{14d}$$

$$\boldsymbol{F}_\omega = \begin{pmatrix} (m_s[\boldsymbol{\omega}_{\text{obj}}]^\times[\boldsymbol{\omega}_{\text{obj}}]^\times \boldsymbol{r}_s - m_s[\boldsymbol{r}_s]^\times \dot{\boldsymbol{S}}_{\text{obj}} \dot{\boldsymbol{\delta}}_{\text{obj}})^T \\ \left\{\boldsymbol{S}_{\text{obj}}^T[[\boldsymbol{\omega}_{\text{obj}}]^\times \boldsymbol{I}_G \boldsymbol{\omega}_{\text{obj}} + [\boldsymbol{\omega}_{\text{obj}}]^\times \boldsymbol{L}_s + (\boldsymbol{I}_G + \boldsymbol{I}_s)\dot{\boldsymbol{S}}_{\text{obj}} \dot{\boldsymbol{\delta}}_{\text{obj}} + m_s[\boldsymbol{r}_s]^\times[\boldsymbol{\omega}_{\text{obj}}]^\times[\boldsymbol{\omega}_{\text{obj}}]^\times \boldsymbol{r}_s]\right\}^T \end{pmatrix} \tag{14e}$$

$$\boldsymbol{G} = \begin{bmatrix} \mathbf{1}_{3\times 3} & \mathbf{0}_{3\times 3} & \cdots & \mathbf{1}_{3\times 3} & \mathbf{0}_{3\times 3} \\ \boldsymbol{S}_{\text{obj}}^T\left[\boldsymbol{r}_e^{(1)}\right]_{3\times 3}^\times & \boldsymbol{S}_{\text{obj}}^T & & \boldsymbol{S}_{\text{obj}}^T\left[\boldsymbol{r}_e^{(n)}\right]_{3\times 3}^\times & \boldsymbol{S}_{\text{obj}}^T \end{bmatrix}_{6\times 6n} \tag{14f}$$

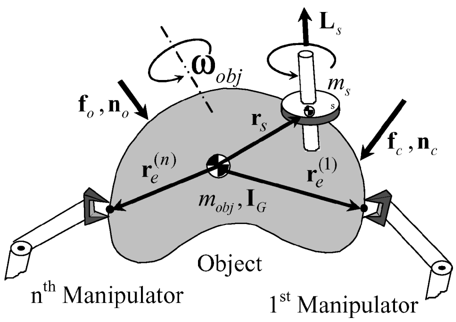

Fig. 2 Object with an internal angular momentum source, manipulated by cooperating manipulators.

where **1** and **0** denote the identity and zero matrices, respectively. The matrix $\boldsymbol{S}_{\text{obj}}$ relates the object angular velocity and the corresponding Euler rates as

$$\boldsymbol{\omega}_{\text{obj}} = \boldsymbol{S}_{\text{obj}}\dot{\boldsymbol{\delta}}_{\text{obj}} \tag{15}$$

For a flexible object an appropriate dynamics model can be simply substituted for the preceding model of a rigid object [Eq. (6)]. Next, the MIC law is developed.

C. MIC Law

A desired impedance law for the object motion can be chosen as

$$\boldsymbol{M}_{\text{des}}\ddot{\boldsymbol{e}} + \boldsymbol{K}_d\dot{\boldsymbol{e}} + \boldsymbol{K}_p\boldsymbol{e} = -\boldsymbol{F}_c \tag{16}$$

Then, considering the target impedance, the required end-effector forces/torques on the object are obtained using Eq. (6) as

$$\boldsymbol{F}_{e_{\text{req}}} = \boldsymbol{G}^{\#}\left[\boldsymbol{M}\boldsymbol{M}_{\text{des}}^{-1}(\boldsymbol{M}_{\text{des}}\ddot{\boldsymbol{X}}_{\text{des}} + \boldsymbol{K}_d\dot{\boldsymbol{e}} + \boldsymbol{K}_p\boldsymbol{e} + \boldsymbol{F}_c) + \boldsymbol{F}_{\omega} - (\boldsymbol{F}_c + \boldsymbol{F}_0)\right] \tag{17}$$

where $\boldsymbol{G}^{\#}$ is defined as

$$\boldsymbol{G}^{\#} = \boldsymbol{W}^{-1}\boldsymbol{G}^T(\boldsymbol{G}\boldsymbol{W}^{-1}\boldsymbol{G}^T)^{-1} \tag{18}$$

Therefore, the controlled forces $\tilde{\boldsymbol{Q}}_f$ in Eq. (5) required to be applied on the manipulated object by the end effectors are

$$\tilde{\boldsymbol{Q}}_f = \begin{Bmatrix} \boldsymbol{0}_{6\times 1} \\ \boldsymbol{F}_{e_{\text{req}}} \end{Bmatrix} \qquad \tilde{\boldsymbol{Q}}_{\text{react}} = \begin{Bmatrix} \boldsymbol{0}_{6\times 1} \\ -\boldsymbol{F}_e \end{Bmatrix} \tag{19}$$

where

$$\boldsymbol{F}_e = \boldsymbol{G}^{\#}[\boldsymbol{M}\ddot{\boldsymbol{X}} + \boldsymbol{F}_{\omega} - (\boldsymbol{F}_c + \boldsymbol{F}_0)] \tag{20}$$

Next, to impose the same impedance law on the spacecraft motion, manipulators, and the object, the impedance law for the space free flyer is written as

$$\tilde{\boldsymbol{M}}_{\text{des}}\ddot{\tilde{\boldsymbol{e}}}_{\text{des}} + \tilde{\boldsymbol{K}}_d\dot{\tilde{\boldsymbol{e}}} + \tilde{\boldsymbol{K}}_p\tilde{\boldsymbol{e}} + \boldsymbol{U}_{f_c}\boldsymbol{F}_c = \boldsymbol{0}_{N\times 1} \tag{21}$$

where $\tilde{\boldsymbol{e}} = \tilde{\boldsymbol{X}}_{\text{des}} - \tilde{\boldsymbol{X}}$ is the tracking error of the SFFR controlled variables (as opposed to $\boldsymbol{e}$, which describes the object tracking error) and $\tilde{\boldsymbol{M}}_{\text{des}}$, $\tilde{\boldsymbol{K}}_p$, and $\tilde{\boldsymbol{K}}_d$ are $N \times N$ block-diagonal matrices based on $\boldsymbol{M}_{\text{des}}$, $\boldsymbol{k}_p$, and $\boldsymbol{k}_d$, respectively, defined as

$$\tilde{\boldsymbol{M}}_{\text{des}} = \begin{bmatrix} \boldsymbol{M}_{\text{des}} & \boldsymbol{0} & \cdots & \boldsymbol{0} \\ \boldsymbol{0} & \boldsymbol{M}_{\text{des}} & \cdots & \vdots \\ \vdots & \boldsymbol{0} & \ddots & \boldsymbol{0} \\ \boldsymbol{0} & \cdots & \boldsymbol{0} & \boldsymbol{M}_{\text{des}} \end{bmatrix}_{N\times N}, \qquad \boldsymbol{U}_{f_c} = \begin{bmatrix} \boldsymbol{1}_{6\times 6} \\ \vdots \\ \boldsymbol{1}_{6\times 6} \end{bmatrix}_{N\times 6} \tag{22a}$$

$$\tilde{\boldsymbol{K}}_p = \begin{bmatrix} \boldsymbol{k}_p & \boldsymbol{0} & \cdots & \boldsymbol{0} \\ \boldsymbol{0} & \boldsymbol{k}_p & \cdots & \vdots \\ \vdots & \boldsymbol{0} & \ddots & \boldsymbol{0} \\ \boldsymbol{0} & \cdots & \boldsymbol{0} & \boldsymbol{k}_p \end{bmatrix}_{N\times N}$$

$$\tilde{\boldsymbol{K}}_d = \begin{bmatrix} \boldsymbol{k}_d & \boldsymbol{0} & \cdots & \boldsymbol{0} \\ \boldsymbol{0} & \boldsymbol{k}_d & \cdots & \vdots \\ \vdots & \boldsymbol{0} & \ddots & \boldsymbol{0} \\ \boldsymbol{0} & \cdots & \boldsymbol{0} & \boldsymbol{k}_d \end{bmatrix}_{N\times N} \tag{22b}$$

The desired trajectory for the system controlled variables $\tilde{\boldsymbol{X}}_{\text{des}}$ can be defined based on the desired trajectory for the object motion $\boldsymbol{X}_{\text{des}}$ and the grasp condition. Then, similar to the derivation for $\tilde{\boldsymbol{Q}}_f$ and assuming that the system mass and geometric parameters are known, $\tilde{\boldsymbol{Q}}_m$ can be obtained as

$$\tilde{\boldsymbol{Q}}_m = \tilde{\boldsymbol{H}}\tilde{\boldsymbol{M}}_{\text{des}}^{-1}\left(\tilde{\boldsymbol{M}}_{\text{des}}\ddot{\tilde{\boldsymbol{X}}}_{\text{des}} + \tilde{\boldsymbol{K}}_d\dot{\tilde{\boldsymbol{e}}} + \tilde{\boldsymbol{K}}_p\tilde{\boldsymbol{e}} + \boldsymbol{U}_{f_c}\boldsymbol{F}_c\right) + \tilde{\boldsymbol{C}} \tag{23}$$

Substituting these results into Eq. (5) makes all participating manipulators, the free-flyer base, and the manipulated object exhibit the same impedance behavior and guarantees an accordant motion of the various subsystems during object manipulation tasks. It was assumed that the exact value of the contact force is available, whereas usually substitution of an estimated value for this, as will be discussed later, is required. Also, mass and geometric properties for the manipulated object, spacecraft, and manipulating arms are assumed to be known, a reasonable assumption for space man-made systems. Finally, it should be mentioned that inspired by the human control system a related formulation to fulfill desired force tracking tasks has been presented in Ref. 32.

D. Error Dynamics

In this section, error dynamics is studied to show that under the MIC law all participating manipulators, the free-flying base, and the manipulated object exhibit the same designated impedance behavior. Hence, an accordant motion of the manipulators and payload is achieved, and the MIC algorithm imposes a consistent motion of all parts of the system. To this end, substituting Eqs. (23) and (19) into Eq. (5) and the result into Eq. (4) yields

$$\tilde{\boldsymbol{H}}(\boldsymbol{q})\left[\tilde{\boldsymbol{M}}_{\text{des}}^{-1}\left(\tilde{\boldsymbol{M}}_{\text{des}}\ddot{\tilde{\boldsymbol{x}}}_{\text{des}} + \tilde{\boldsymbol{k}}_d\dot{\tilde{\boldsymbol{e}}} + \tilde{\boldsymbol{k}}_p\tilde{\boldsymbol{e}} + \boldsymbol{U}_{f_c}\boldsymbol{F}_c\right) - \ddot{\tilde{\boldsymbol{x}}}\right] + \begin{Bmatrix} \boldsymbol{0}_{6\times 1} \\ \boldsymbol{G}^{\#}\boldsymbol{M}\left[\boldsymbol{M}_{\text{des}}^{-1}(\boldsymbol{M}_{\text{des}}\ddot{\boldsymbol{x}}_{\text{des}} + \boldsymbol{k}_d\dot{\boldsymbol{e}} + \boldsymbol{k}_p\boldsymbol{e} + \boldsymbol{F}_c) - \ddot{\boldsymbol{x}}\right] \end{Bmatrix} = \boldsymbol{0} \tag{24}$$

Because Eq. (24) must hold for any $\boldsymbol{M}$ and $\tilde{\boldsymbol{H}}$, it can be concluded that

$$\tilde{\boldsymbol{H}}(\boldsymbol{q})\left[\tilde{\boldsymbol{M}}_{\text{des}}^{-1}\left(\tilde{\boldsymbol{M}}_{\text{des}}\ddot{\tilde{\boldsymbol{x}}}_{\text{des}} + \tilde{\boldsymbol{k}}_d\dot{\tilde{\boldsymbol{e}}} + \tilde{\boldsymbol{k}}_p\tilde{\boldsymbol{e}} + \boldsymbol{U}_{f_c}\boldsymbol{F}_c\right) - \ddot{\tilde{\boldsymbol{x}}}\right] = \boldsymbol{0}$$

$$\boldsymbol{G}^{\#}\boldsymbol{M}\left[\boldsymbol{M}_{\text{des}}^{-1}(\boldsymbol{M}_{\text{des}}\ddot{\boldsymbol{x}}_{\text{des}} + \boldsymbol{k}_d\dot{\boldsymbol{e}} + \boldsymbol{k}_p\boldsymbol{e} + \boldsymbol{F}_c) - \ddot{\boldsymbol{x}}\right] = \boldsymbol{0} \tag{25}$$

Now, based on Eqs. (14f) and (18) it can be seen that the pseudoinverse of the grasp matrix $\boldsymbol{G}^{\#}$ is a full-rank matrix. Therefore, Eq. (25) results in

$$\tilde{\boldsymbol{H}}(\boldsymbol{q})\left[\tilde{\boldsymbol{M}}_{\text{des}}^{-1}\left(\tilde{\boldsymbol{M}}_{\text{des}}\ddot{\tilde{\boldsymbol{x}}}_{\text{des}} + \tilde{\boldsymbol{k}}_d\dot{\tilde{\boldsymbol{e}}} + \tilde{\boldsymbol{k}}_p\tilde{\boldsymbol{e}} + \boldsymbol{U}_{f_c}\boldsymbol{F}_c\right) - \ddot{\tilde{\boldsymbol{x}}}\right] = \boldsymbol{0}$$

$$\boldsymbol{M}\left[\boldsymbol{M}_{\text{des}}^{-1}(\boldsymbol{M}_{\text{des}}\ddot{\boldsymbol{x}}_{\text{des}} + \boldsymbol{k}_d\dot{\boldsymbol{e}} + \boldsymbol{k}_p\boldsymbol{e} + \boldsymbol{F}_c) - \ddot{\boldsymbol{x}}\right] = \boldsymbol{0} \tag{26}$$

Finally, based on the fact that $\boldsymbol{M}$ and $\tilde{\boldsymbol{H}}$ are positive-definite inertia matrices, Eq. (26) results in

$$\tilde{\boldsymbol{M}}_{\text{des}}\ddot{\tilde{\boldsymbol{e}}}_{\text{des}} + \tilde{\boldsymbol{K}}_d\dot{\tilde{\boldsymbol{e}}} + \tilde{\boldsymbol{K}}_p\tilde{\boldsymbol{e}} + \boldsymbol{U}_{f_c}\boldsymbol{F}_c = \boldsymbol{0}$$

$$\boldsymbol{M}_{\text{des}}\ddot{\boldsymbol{e}} + \boldsymbol{K}_d\dot{\boldsymbol{e}} + \boldsymbol{K}_p\boldsymbol{e} + \boldsymbol{F}_c = \boldsymbol{0} \tag{27}$$

which means that all participating manipulators, the free-flyer base, and the manipulated object exhibit the same impedance behavior. Next, the estimation procedure for the contact force is discussed.

E. Contact Force Estimation

As mentioned in the preceding section, computation of $\boldsymbol{F}_{e_{\mathrm{req}}}$ requires knowing the value of the contact force $\boldsymbol{F}_c$. Normally, this has to be estimated, which is discussed here.

Equation (6) can be rewritten as

$$\boldsymbol{F}_c = \boldsymbol{M}\ddot{\boldsymbol{x}} + \boldsymbol{F}_\omega - \boldsymbol{F}_0 - \boldsymbol{G}\boldsymbol{F}_e \tag{28}$$

It is assumed that the external forces/torques $\boldsymbol{F}_0$ and also the object mass and geometric properties are known. Assuming that end effectors are equipped with force sensors, $\boldsymbol{F}_e$ can be measured and substituted into Eq. (28). Also, based on the measurements of object motion $\boldsymbol{F}_\omega$ can be computed and substituted into Eq. (28). However, to evaluate the contact force the object acceleration has to be known, too. Because this is not usually available, it has to be approximated through a numerical procedure. To implement object impedance control, Schneider and Cannon[26] suggest either to use the desired acceleration, or to use the last commanded acceleration, defined as

$$\ddot{\boldsymbol{x}}_{\mathrm{cmd}} = \boldsymbol{M}_{\mathrm{des}}^{-1}(\boldsymbol{M}_{\mathrm{des}}\ddot{\boldsymbol{x}}_{\mathrm{des}} + \boldsymbol{k}_d\dot{\boldsymbol{e}} + \boldsymbol{k}_p\boldsymbol{e} + \hat{\boldsymbol{F}}_c) \tag{29}$$

They describe that both of these two approximations yield acceptable experimental results, though it has been emphasized that a more sophisticated procedure would improve the performance. Because there might be a considerable difference between $\ddot{\boldsymbol{x}}$ and $\ddot{\boldsymbol{x}}_{\mathrm{des}}$, particularly after contact the first approach does not yield a reliable approximation. The second approach can result in a poor approximation because of sudden variations at each contact.

Here, the approach taken is to use directly a finite difference approximation as

$$\ddot{\hat{\boldsymbol{x}}} = \frac{\dot{\boldsymbol{x}}_t - \dot{\boldsymbol{x}}_{t-\Delta t}}{\Delta t} \tag{30a}$$

or

$$\ddot{\hat{\boldsymbol{x}}} = \frac{\boldsymbol{x}_t - 2\boldsymbol{x}_{t-\Delta t} + \boldsymbol{x}_{t-2\Delta t}}{(\Delta t)^2} \tag{30b}$$

where Δt is the time step used in the estimation procedure. Because of practical reasons (i.e., time requirement for measurements and corresponding calculations), Δt cannot be infinitesimally close to zero. In practice, a sufficiently small Δt can be employed so that the resulting errors are negligible, even at the time of contact. Substituting Eq. (30) for acceleration, the contact force can be estimated from Eq. (28) as

$$\hat{\boldsymbol{F}}_c = \boldsymbol{M}\ddot{\hat{\boldsymbol{x}}} + \boldsymbol{F}_\omega - \boldsymbol{F}_0 - \boldsymbol{G}\boldsymbol{F}_e \tag{31}$$

Next, the disturbance rejection characteristics of the MIC algorithm are studied.

III. Disturbance Rejection Analysis

The effects of disturbances that are applied on several arbitrary points of a SFFR are considered here. The resultant generalized disturbance can be described as[33]

$$\boldsymbol{Q}_{\mathrm{dist}} = -\sum_{j=1}^{n_f} \boldsymbol{J}_i^{(m)^T} \boldsymbol{Q}_{\mathrm{dist}_i j}^{(m)} \tag{32}$$

where the Jacobian matrix $\boldsymbol{J}_i^{(m)}$ is a $6 \times \boldsymbol{N}$ matrix defined as

$$\begin{Bmatrix} \dot{\boldsymbol{R}}_i \\ \boldsymbol{\omega}_i^{(m)} \end{Bmatrix} = \boldsymbol{J}_i^{(m)}\dot{\boldsymbol{q}} \tag{33}$$

which relates the generalized velocities $\dot{\boldsymbol{q}}$ to the linear velocity $\dot{\boldsymbol{R}}_i$ and angular velocity $\boldsymbol{\omega}_i^{(m)}$ of the exerted body. The generalized disturbance, as described in Eq. (32) in the joint space, can be expressed in the task space as

$$\tilde{\boldsymbol{Q}}_{\mathrm{dist}} = \left(\boldsymbol{J}_c^T\right)^{-1}\boldsymbol{Q}_{\mathrm{dist}} \tag{34}$$

where the Jacobian matrix $\boldsymbol{J}_c$ is defined as

$$\dot{\tilde{\boldsymbol{X}}} = \boldsymbol{J}_c\dot{\boldsymbol{q}} \tag{35}$$

Therefore, the vector of generalized forces in the task space $\tilde{\boldsymbol{Q}}$, as given in Eq. (5), will be obtained as

$$\tilde{\boldsymbol{Q}} = \tilde{\boldsymbol{Q}}_m + \tilde{\boldsymbol{Q}}_f + \tilde{\boldsymbol{Q}}_{\mathrm{react}} + \tilde{\boldsymbol{Q}}_{\mathrm{dist}} \tag{36}$$

Noting the fact that $\tilde{\boldsymbol{Q}}_{\underset{\sim}{f}}$ is virtually canceled by the reaction load on each end effector $\tilde{\boldsymbol{Q}}_{\mathrm{react}}$ and substituting Eq. (36) into Eq. (4), Eq. (37) is obtained:

$$\tilde{\boldsymbol{H}}(\boldsymbol{q})\ddot{\tilde{\boldsymbol{X}}} + \tilde{\boldsymbol{C}}(\boldsymbol{q},\dot{\boldsymbol{q}}) = \tilde{\boldsymbol{Q}}_m + \tilde{\boldsymbol{Q}}_{\mathrm{dist}} \tag{37}$$

Next, substituting Eq. (23) into Eq. (37), Eq. (38) can be obtained:

$$\begin{aligned}\tilde{\boldsymbol{H}}(\boldsymbol{q})\tilde{\boldsymbol{M}}_{\mathrm{des}}^{-1}&\left(\tilde{\boldsymbol{M}}_{\mathrm{des}}\ddot{\tilde{\boldsymbol{X}}}_{\mathrm{des}} + \tilde{\boldsymbol{K}}_d\dot{\tilde{\boldsymbol{e}}} + \tilde{\boldsymbol{K}}_p\tilde{\boldsymbol{e}} + \boldsymbol{U}_{f_c}\boldsymbol{F}_c\right)\\ &+ \tilde{\boldsymbol{C}}(\boldsymbol{q},\dot{\boldsymbol{q}}) + \tilde{\boldsymbol{Q}}_{\mathrm{dist}} = \tilde{\boldsymbol{H}}(\boldsymbol{q})\ddot{\tilde{\boldsymbol{X}}} + \tilde{\boldsymbol{C}}(\boldsymbol{q},\dot{\boldsymbol{q}})\end{aligned} \tag{38}$$

which can be simplified to

$$\tilde{\boldsymbol{M}}_{\mathrm{des}}\ddot{\tilde{\boldsymbol{e}}}_{\mathrm{des}} + \tilde{\boldsymbol{K}}_d\dot{\tilde{\boldsymbol{e}}} + \tilde{\boldsymbol{K}}_p\tilde{\boldsymbol{e}} + \boldsymbol{U}_{f_c}\boldsymbol{F}_c = -\tilde{\boldsymbol{M}}_{\mathrm{des}}\tilde{\boldsymbol{H}}^{-1}(\boldsymbol{q})\tilde{\boldsymbol{Q}}_{\mathrm{dist}} \tag{39}$$

As it is seen, the resultant disturbing torque/force appears in the right-hand side of the whole system error equation. Noting the fact that the inertia matrix $\tilde{\boldsymbol{H}}(\boldsymbol{q})$ is a positive-definite matrix, it can be guaranteed that $\tilde{\boldsymbol{H}}^{-1}(\boldsymbol{q})$ remains bounded. As expected from physical intuition, Eq. (39) reveals that increasing the mass properties of SFFR reduces the effects of disturbances. Also, the desired mass matrix appears as a coefficient in the right-hand side of Eq. (39). This means that one can reduce the effects of disturbances by choosing lower values for the elements of $\tilde{\boldsymbol{M}}_{\mathrm{des}}$. By decreasing the values for the elements of $\tilde{\boldsymbol{M}}_{\mathrm{des}}$, the system behaves with lower inertia and its response becomes faster.

Next, to examine the developed MIC law a system of three appendages mounted on a space free flyer is simulated.

IV. Simulation Results

As shown in Fig. 3, a system of two manipulators mounted on a space free flyer is simulated in this section, in which a third appendage is considered as a communication antenna. A remote center compliance (RCC) is attached to the second end effector, as shown in Fig. 3, to consider practical aspects and also to show the capability of the MIC law in the presence of system flexibility. (A RCC is a compliant structure between the wrist of a manipulator and its end

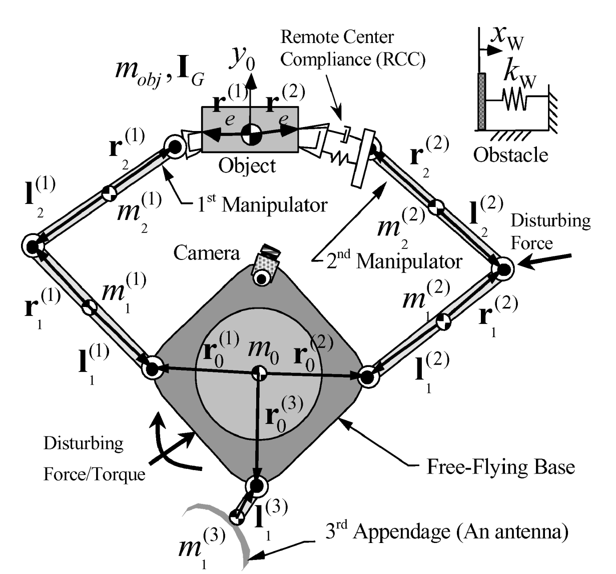

Fig. 3 Simulated SFFR performing a cooperative object manipulation task, under the effect of disturbing forces/torques.

tool. Hence, the RCC is essentially an arrangement of springs that makes it possible for a manipulator to perform contact tasks without difficulty or damaging different system parts, for example, inserting a pin into a hole can be performed even though the clearance between the pin and hole is such that the manipulator would not be normally able to place the pin into that.[34]) The SFFR performs a cooperative manipulation task, that is, moving an object with two manipulators according to predefined trajectories, and is subject to significant force and torque disturbances at several points. As shown in Fig. 3, the antenna is connected to the base of the system and should keep a constant absolute orientation toward a remote center.

For illustration purposes, the desired trajectory for the object is planned such that it passes through an obstacle, and the object has to come to a smooth stop at the obstacle. The object has been grabbed with a pivoted grasp condition, that is, no torque can be exerted on the object by the two end effectors. The initial conditions, system geometric parameters, mass properties, and the maximum available actuator torques and forces of system base, antenna, cooperative manipulators, and manipulated object have been presented in the Appendix.

The system dynamics model of the described SFFR is a central element in the simulation code, using a barycentric method and MAPLE tools. The code (SPACEMAPLE) yields the mass matrix $\boldsymbol{H}$, the vector of nonlinear velocity terms $\boldsymbol{C}$ (both in the joint space and task space), also the Jacobian matrix and its time derivative, each one as an analytical function of generalized coordinates and speeds.[30] Next, the dynamics model in a symbolic (analytical) format is imported to the simulation routine in MATLAB®, where equations of motion under the developed MIC law are integrated, using the Gear algorithm.

The obstacle is at $x_w = 3.1$ m, and so it is expected that the object will come into contact at its right side. Therefore, as seen in the following simulation results, the contact occurs at $t \approx 7.5$ s along the x direction, so that no contact force affects the object motion in the y direction. After the contact, because the x position depends on the dynamics of the environment, according to the impedance law, the base smoothly comes back until position converges to a final value, which is determined by the desired contact force on the obstacle. It is assumed that no torque is developed at the contact surface (i.e., a point contact occurs); therefore, $\boldsymbol{n}_c$ is equal to the moment of $\boldsymbol{f}_c$. Also, there is no other external force applied on the object, that is, $\boldsymbol{f}_0 = \boldsymbol{0}$, $\boldsymbol{n}_0 = \boldsymbol{0}$. The contact force is calculated based on the real stiffness of the obstacle, which is $k_w = 1e5$ N/m. The desired trajectories for the object and base center of mass, expressed in the inertial frame, are chosen as

$$x_{\mathrm{des}_0} = -0.1791 + 4(1 - e^{-0.2t}) \quad \text{(m)}$$

$$x_{\mathrm{des}_{\mathrm{base}}} = 0.025 + 3(1 - e^{-0.2t}) \quad \text{(m)}$$

$$y_{\mathrm{des}_0} = 0.4 \quad \text{(m)}, \qquad y_{\mathrm{des}_{\mathrm{base}}} = -0.03 \quad \text{(m)}$$

where the origin of the inertial frame is considered to be located at the system center of mass at initial time.

The controller gains are chosen as

$$\boldsymbol{K}_p = \mathrm{diag}(100, \ldots, 100) \quad (\mathrm{kgS}^{-2})$$

$$\boldsymbol{K}_d = \mathrm{diag}(20, \ldots, 20) \quad (\mathrm{kgS}^{-1})$$

First, to see the effect of mass matrix gain on the system behavior, no disturbances are considered, and the system performance is simulated in three cases, that is, different selections of the desired mass matrix $\boldsymbol{M}_{\mathrm{des}} = \mathrm{diag}(1, \ldots, 1)$, $\boldsymbol{M}_{\mathrm{des}} = \mathrm{diag}(0.5, \ldots, 0.5)$, and $\boldsymbol{M}_{\mathrm{des}} = \mathrm{diag}(0.2, \ldots, 0.2)$. As shown in Fig. 4, by decreasing the values of controller mass matrix elements the y component of the object position tracking error remains very close to zero before the contact and eventually vanishes after that. Note that the contact occurs along the x direction, at $t \approx 7.5$ s, so that does not affect the object motion in the y direction. Other position tracking errors, that is, free-flying base and the two manipulators end effectors, are very similar to the object position tracking errors. Also, decreasing the values of controller mass matrix elements has a similar effect on the rate of these errors and results in a smoother tracking. Consequently, the contact force estimation procedure, which is based on finite difference calculation of the object acceleration, yields more accurate results. Therefore, as shown in Fig. 4, when no disturbances are applied on the system, decreasing the values of controller mass matrix elements has minor improving effects on the system performance.

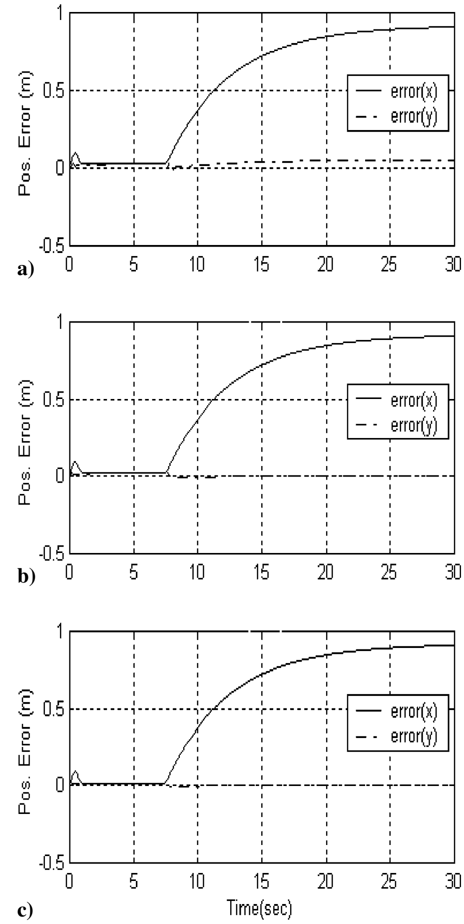

Fig. 4 Object position tracking error when no disturbing forces/torques are applied: a) $\boldsymbol{M}_{\mathrm{des}} = \mathrm{diag}(1, \ldots, 1)$, b) $\boldsymbol{M}_{\mathrm{des}} = \mathrm{diag}(0.5, \ldots, 0.5)$, and c) $\boldsymbol{M}_{\mathrm{des}} = \mathrm{diag}(0.2, \ldots, 0.2)$.

To see disturbance rejection characteristics for the developed MIC law, disturbing forces/torques of step type equal to [50 N, 50 N, 50 N · m] are applied on the free-flyer base at a distance of [0.5, 0.5] in its body coordinate, when it reaches to $x = 1.5$ m in the inertial frame. Another disturbing force equal to [50 N, 50 N] is applied on the second joint of the second manipulator, as depicted in Fig. 3. Note that these disturbances are significant, compared to the base actuator saturation limits. The system performance is now simulated for the two selections of $\boldsymbol{M}_{\mathrm{des}} = \mathrm{diag}(0.15, \ldots, 0.15)$ and $\boldsymbol{M}_{\mathrm{des}} = \mathrm{diag}(1.0, \ldots, 1.0)$, and the results are depicted in Fig. 5.

As shown in Fig. 5a, the y component of the object position tracking error remains very close to zero before the contact and eventually vanishes after that. This is because the contact occurs along the x direction, so that it does not affect the object motion in the y direction. Other position tracking errors, that is, free-flying base position errors and manipulator end effectors, and the rate of these errors behave similarly to the object position tracking errors. On the other hand, the x component of error, starting from some initial value, decreases at some rate till contact occurs, at $t \approx 7.5$ s (Fig. 5). This rate changes after contact because the tracking error dynamics depends on the dynamics of the environment, according to the impedance law. Then, this error smoothly converges to the distance between the final desired x position and the obstacle x position.

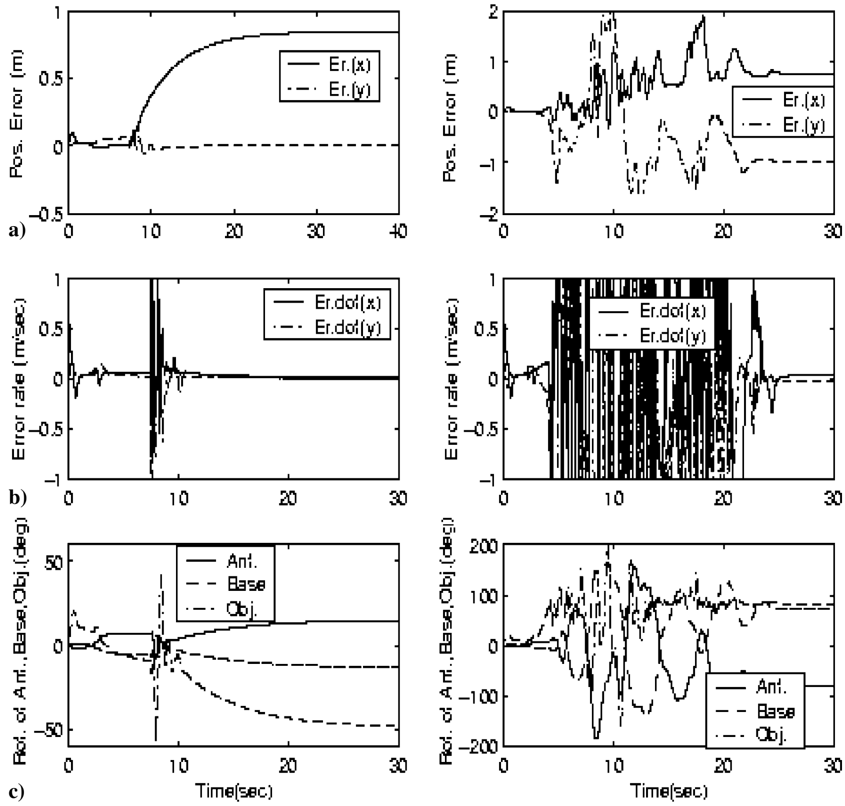

Fig. 5 Disturbing forces/torques are applied on the base and manipulator: left, $M_{\text{des}} = \text{diag}(0.15, \ldots, 0.15)$ and right, $M_{\text{des}} = \text{diag}(1.0, \ldots, 1.0)$: a) object position tracking error, b) rate of tracking error, and c) orientation tracking error.

As discussed in the preceding section, decreasing the values of controller mass matrix has a substantial effect on the error dynamics. As seen in Fig. 5, lower values of controller mass matrix elements (corresponding to the left-hand side of the figure) result in smaller object tracking error, as do other position tracking errors. The orientation error starting from zero grows to some amount until contact occurs, and then it converges to a final limited value. The initial growth is because the first end effector (i.e., without the RCC unit) responds faster than the second one. Therefore, the difference between the two end-effector forces produces some couples that results in an undesirable rotation of the object. Because there is no direct control on the object orientation, as a result of the pivoted grasp condition, the object orientation converges to a final limited value. As seen in Fig. 5, the object position error and its time derivative, also other errors in rotation of base, antenna, and all manipulator end effectors decrease by reducing the values of desired mass matrix. The simulation results reveal the merits of the MIC algorithm in terms of suitably smooth performance, that is, proper tracking errors in the presence of impacts caused by contact with the obstacle and also significant disturbances.

V. Conclusions

In this paper, the MIC law was formulated and applied to space robotic systems. In space, participating robotic arms are connected through a free-flying base, and the formulation had to consider the dynamic coupling between the arms and the base. For the manipulated object, inclusion of an internal source of angular momentum was admitted, as is the case for most satellite manipulation tasks. By error analysis, it was shown that under the MIC law all participating manipulators, the free-flyer base, and the manipulated object exhibit the same designed impedance behavior. Next, the disturbance rejection characteristics of the MIC law applied to a SFFR in manipulating an object was studied. It was shown that increasing the mass properties of SFFR, which is an inherent characteristic of the system, reduces the effects of disturbances. It was also shown that the effect of disturbances can be substantially decreased by appropriate tuning of the controller mass matrix gain. Finally, to examine the developed MIC law a system of three appendages mounted on a space free flyer was simulated. Based on the simulation results the merits of the MIC algorithm in terms of disturbance rejection characteristics was revealed, that is, negligible small tracking errors can be achieved in the presence of significant disturbing forces/torques. This is because, based on the MIC law, all participating manipulators, the free-flyer base, and the manipulated object exhibit the same impedance behavior, which guarantees an accordant motion of the various subsystems during object manipulation tasks.

Appendix: Initial Conditions and System Parameters

The initial conditions and parameters for the simulated system, as depicted in Fig. 3, are summarized here. The SFFR parameters are described in Tables A1–A3. The initial conditions are chosen as

$$\boldsymbol{q} = \left(x_{\text{cm}_s}, y_{\text{cm}_s}, \delta_0, \theta_{11}, \theta_{12}, \theta_{21}, \theta_{22}, \theta_{31}, \theta_{\text{obj}}\right)$$

$$= (0.0, 0.0, 0.0, 2.7, -2.7, 1.0, 2.5, 0.0, 0.0) \quad (\text{m, rad})$$

$$\dot{\boldsymbol{q}} = \boldsymbol{0}$$

The stiffness and damping properties of the RCC unit are chosen as follows,[35] where it is assumed that it is initially free of tension or compression:

$$\boldsymbol{k}_e = \text{diag}(1.2, 1.2) \times 10^3\ \text{kgs}^{-1}$$

$$\boldsymbol{b}_e = \text{diag}(5, 5) \times 10^2\ \text{kgs}^{-2}$$

Table A1 Base parameters and saturation limits

Parameter	Value
$r_0^{(1)}$, m	0.5
$r_0^{(2)}$, m	0.5
$r_0^{(3)}$, m	0.5
m_0, kg	50
I_0, $\mathrm{kg \cdot m^2}$	10
F_x, N	100
F_y, N	100
τ_0, $\mathrm{N \cdot m}$	20

Table A2 Manipulators parameters and limits

No.	ith body	$r_i^{(m)}$, m	$l_i^{(m)}$, m	$m_i^{(m)}$, kg	$I_i^{(m)}$, $\mathrm{kg \cdot m^2}$	$\boldsymbol{\tau}_i^{(m)}$, $\mathrm{N \cdot m}$
1	1	0.50	0.50	4.0	0.50	70
1	2	0.50	0.50	3.0	0.25	70
2	1	0.50	0.50	4.0	0.50	70
2	2	0.50	0.50	3.0	0.25	70
3	1	0.25	0.25	5.0	2.00	70

Table A3 Manipulated object parameters

Parameter	Value
m_0, kg	3.0
I_0, $\mathrm{kg \cdot m^2}$	0.5
$r_e^{(1)}$, m	0.2
$r_e^{(2)}$, m	0.2

References

[1]Jacobsen, S., Lee, C., Zhu, C., and Dubowsky, S., "Planning of Safe Kinematic Trajectories for Free Flying Robots Approaching an Uncontrolled Spinning Satellite," *Proceedings of ASME Design Engineering Technical Conferences and Computer and Information in Engineering Conference*, 2002.

[2]Vafa, Z., and Dubowsky, S., "On The Dynamics of Manipulators in Space Using the Virtual Manipulator Approach," *Proceedings of IEEE International Conference on Robotics and Automation*, 1987, pp. 579–585.

[3]Xu, Y., "The Measure of Dynamic Coupling of Space Robot Systems," *Proceedings of IEEE International Conference on Robotics and Automation*, 1993, pp. 615–620.

[4]Moosavian, S. A. A., and Papadopoulos, E., "On the Kinematics of Multiple Manipulator Space Free-Flyers and Their Computation," *Journal of Robotic Systems*, Vol. 15, No. 4, 1998, pp. 207–216.

[5]Moosavian, S. A. A., and Papadopoulos, E., "Coordinated Motion Control of Multiple Manipulator Space Free-Flyers," *Advances in the Astronautical Sciences*, Vol. 95, Pt. 1, 1997, pp. 501–516.

[6]Umetani, Y., and Yoshida, K., "Resolved Motion Control of Space Manipulators with Generalized Jacobian Matrix," *IEEE Transactions on Robotics and Automation*, Vol. 5, No. 3, 1989, pp. 303–314.

[7]Alexander, H., and Cannon, R., "An Extended Operational Space Control Algorithm for Satellite Manipulators," *The Journal of the Astronautical Sciences*, Vol. 38, No. 4, 1990, pp. 473–486.

[8]Dubowsky, S., and Papadopoulos, E., "The Dynamics and Control of Space Robotic Systems," *IEEE Transactions on Robotics and Automation*, Vol. 9, No. 5, 1993, pp. 531–543.

[9]Wee, L. B., and Walker, M. W., "On the Dynamics of Contact Between Space Robots and Configuration Control for Impact Minimization," *IEEE Transactions on Robotics and Automation*, Vol. 9, No. 5, 1993, pp. 581–591.

[10]Nakamura, Y., and Mukherjee, R., "Exploiting Nonholonomic Redundancy of Free-Flying Space Robots," *IEEE Transactions on Robotics and Automation*, Vol. 9, No. 4, 1993, pp. 499–506.

[11]Papadopoulos, E., and Moosavian, S. A. A., "Dynamics & Control of Space Free-Flyers with Multiple Arms," *Journal of Advanced Robotics*, Vol. 9, No. 6, 1995, pp. 603–624.

[12]Taniwaki, S., Matunaga, S., Tsurumi, S., and Ohkami, Y., "Coordinated Control of a Satellite-Mounted Manipulator with Consideration of Payload Flexibility," *Journal of Control Engineering Practice*, Vol. 9, No. 2, 2001, pp. 207–215.

[13]Rutkovsky, V. Y., Sukhanov, V. M., Glumov, V. M., Zemlyakov, S. D., and Dodds, S. D., "Computer Simulation of an Adaptive Control System for a Free-Flying Space Robotic Module with Flexible Payload's Transportation," *Journal of Mathematics and Computers in Simulation*, Vol. 58, No. 3, 2002, pp. 407–421.

[14]Inaba, N., Nishimaki, T., Asano, M., and Oda, M., "Rescuing a Stranded Satellite in Space-Experimental Study of Satellite Captures Using a Space Manipulator," *Proceedings of IEEE/RSJ International Conference on Intelligent Robots and Systems*, 2003, pp. 3071–3076.

[15]Yoshida, K., and Nakanishi, H., "Impedance Matching in Capturing a Satellite by a Space Robot," *IEEE/RSJ International Conference on Intelligent Robots and Systems*, 2003, pp. 3059–3064.

[16]Raibert, M. H., and Craig, J. J., "Hybrid Position/Force Control of Manipulators," *Journal of Dynamic Systems, Measurement and Control*, Vol. 126, No. 2, 1981, pp. 126–133.

[17]Hayati, S., "Hybrid Position/Force Control of Multi-Arm Cooperating Robots," *Proceedings of the IEEE International Conference on Robotics and Automation*, 1986, pp. 82–89.

[18]Hogan, N., "Impedance Control: An Approach to Manipulation," *Journal of Dynamic Systems, Measurement and Control*, Vol. 107, No. 1, 1985, pp. 1–24.

[19]Goldenberg, A. A., "Implementation of Force and Impedance Control in Robot Manipulators," *Proceedings of the IEEE International Conference on Robotics and Automation*, 1988, pp. 1626–1632.

[20]Jung, S., and Hsia, T. C., "Stability and Convergence Analysis of Robust Adaptive Force Tracking Impedance Control of Robot Manipulators," *Proceedings of the IEEE/RSJ International Conference on Intelligent Robots and Systems*, 1999, pp. 635–640.

[21]Arimoto, S., Han, H. Y., Cheah, C. C., and Kawamura, S., "Extension of Impedance Matching to Nonlinear Dynamics of Robotic Tasks," *Journal of Systems and Control Letters*, Vol. 36, No. 2, 1999, pp. 109–119.

[22]Caccavale, F., Chiacchio, P., and Chiaverini, S., "Task-Space Regulation of Cooperative Manipulators," *Automatica*, Vol. 36, No. 6, 2000, pp. 879–887.

[23]Caccavale, F., and Villani, L., "An Impedance Control Strategy for Cooperative Manipulation," *Proceedings of the IEEE/ASME International Conference on Advanced Intelligent Mechatronics*, 2001, pp. 343–348.

[24]Biagiotti, L., Liu, H., Hirzinger, G., and Melchiorri, C., "Cartesian Impedance Control for Dexterous Manipulation," *Proceedings of IEEE/RSJ International Conference on Intelligent Robots and Systems*, 2003, pp. 3270–3275.

[25]Ozawa, R., and Kobayashi, H., "A New Impedance Control Concept for Elastic Joint Robots," *Proceedings of the IEEE International Conference on Robotics and Automation*, 2003, pp. 3126–3131.

[26]Schneider, S. A., and Cannon, R. H., "Object Impedance Control for Cooperative Manipulation: Theory and Experimental Results," *IEEE Transactions on Robotics and Automation*, Vol. 8, No. 3, 1992, pp. 383–394.

[27]Meer, D. W., and Rock, S. M., "Coupled System Stability of Flexible-Object Impedance Control," *Proceedings of the IEEE International Conference on Robotics and Automation*, 1995, pp. 1839–1845.

[28]Moosavian, S. A. A., and Papadopoulos, E., "On the Control of Space Free-Flyers Using Multiple Impedance Control," *Proceedings of the IEEE International Conference on Robotics and Automation*, 1997.

[29]Moosavian, S. A. A., and Papadopoulos, E., "Multiple Impedance Control for Object Manipulation," *Proceedings of IEEE/RSJ International Conference on Intelligent Robots and Systems*, 1998, pp. 461–466.

[30]Moosavian, S. A. A., and Papadopoulos, E., "Explicit Dynamics of Space Free-Flyers with Multiple Manipulators via SPACEMAPL," *Journal of Advanced Robotics*, Vol. 18, No. 2, 2004, pp. 223–244.

[31]Meirovitch, L., *Methods of Analytical Dynamics*, McGraw–Hill, New York, 1970, Chap. 4.

[32]Moosavian, S. A. A., and Rastegari, R., "Force Tracking in Multiple Impedance Control of Space Free-Flyers," *Proceedings of IEEE/RSJ International Conference on Intelligent Robots and Systems*, 2000, pp. 1646–1651.

[33]Moosavian, S. A. A., and Rastegari, R., "Disturbance Rejection Analysis of Multiple Impedance Control for Space Free-Flying Robots," *Proceedings of IEEE/RSJ International Conference on Intelligent Robots and Systems*, 2002, pp. 2250–2255.

[34]Craig, J., *Introduction to Robotics, Mechanics and Control*, Addison Wesley Longman, Reading, MA, 1989, Sec. 11.7.

[35]De Fazio, T. L., Seltzer, D. S., and Whitney, D. E., "The Instrumented Remote Centre Compliance," *Journal of the Industrial Robot*, Vol. 11, No. 4, 1984, pp. 238–242.